Acta metall. Vol. 36, No. 4, pp. 925–936, 1988
Printed in Great Britain.

0001-6160/88 $3.00 + 0.00

AN IMPROVED METHOD FOR SHOCK CONSOLIDATION OF POWDERS

M. A. MEYERS and S. L. WANG

Department of Materials and Metallurgical Engineering and Center for Explosives Technology Research, New Mexico Institute of Mining and Technology, Socorro, NM 87801, U.S.A.

(*Received* 18 *October* 1986; *in revised form* 10 *August* 1987)

Abstract—A technique for shock consolidation of powders was developed. This technique uses the cylindrical geometry with two co-axial tubes. The powder is contained in the internal tube. The external tube is surrounded by the explosive charge, which is detonated at one end; this external tube acts as a flyer tube, impacting the internal tube. This technique generates pressures in the powder that can be several times higher than the ones generated by the single-tube technique. The main advantage of this technique is that it allows the use of low detonation-velocity explosives for consolidating hard powders. The lower detonation-velocity explosives minimize cracking of compacts. Significant improvements in compact quality were obtained in nickel-base superalloys, titanium alloys and aluminum–lithium alloys.

Résumé—Nous avons développé une méthode de consolidation par choc des poudres. Cette technique utilise la géométrie cylindrique avec deux tubes coaxiaux. La poudre est contenue dans le tube interne. Le tube externe est entouré par la charge explosive que l'on amorce à l'une des extrémités; ce tube externe agit comme un tube volant tombant sur le tube interne. Cette méthode provoque dans la poudre des pressions plusieurs fois supérieures à celles que crée la méthode à un seul tube: sone principal avantage est de permettre l'utilisation d'explosifs à faible viteese de détonation pour consolider des poudres dures. Les explosifs à vitesse de détonation plus basse diminuent la fissuration des poudres rendues compactes. Nous avons obtenu des améliorations importantes de la qualité des poudres compactées dans le cas de superalliages à base nickel, d'alliages de titane et d'alliages aluminium–lithium.

Zusammenfassung—Ein neues Verfahren zur Stoßverdichtung von Pulvern wird vorgestellt. Hierbei wird eine zylindrische Geometrie mit zwei koachsialen Rohren verwendet. Das Pulver befindet sich im inneren Rohr. Das äußere Rohr ist umgeben von einer Explosivladung. Diese wird an einem Ende gezündet, wodurch das äußere auf das innere Rohr geschossen wird. Mit diesem Verfahren können Drucke auf das Pulver ausgeübt werden, die mehrfach höher sind als diejenigen, die bei dem Einrohrverfahren erreicht werden können. Ein wichtiger Vorteil des Zweirohrverfahrens ist, daß Explosivstoffe mit niedriger Detonationsgeschwindigkeit zur Verdichtung harter Pulver verwendet werden können. Die geringere Detonationsgeschwindigkeit verringert Rißbildung im Preßling. Mit diesem Verfahren konnten deutliche Verbesserungen in der Qualität von Preßlingen aus Superlegierungen auf Nickelbasis, aus Titan- und Aluminium–Lithium-Legierungen erreicht werden.

1. INTRODUCTION

Shock consolidation is a technique that shows considerable promise for producing bulk material from powders [1]. Rapid solidification technology is a rapidly advancing field, and unique microstructures of metallic alloys and ceramics have been created. Shock consolidation is a process by which the particle surfaces are highly deformed (and often molten and resolidified) producing interparticle bonding in a one-step-process. This occurs during the passage of a shock wave through the powder. The two most severe limitations of this process are cracking [1, 2] and net-shape capability [1]. Considerable effort has been devoted to the consolidation of rapidly solidified amorphous and crystalline materials, and successful efforts have been reported by Cline and Hopper [3], Raybould [4], and Morris [5], among others. The past work is reviewed by Gourdin [6] and Prummer [7, 8].

In shock hardening of metals, it is well known that the plate impact technique provides greater pressures than explosives in direct contact with the metal. Shock consolidation of cylinders has, for the most part, been carried out using the explosive in direct contact with the tubular powder container. While this technique gives good consolidates for "soft" powders, such as pure copper and nickel, it is not very successful with "hard" powders. The critical shock parameters governing shock consolidation are pressure, pulse duration, and shock temperature [9]. Material parameters of importance are the powder porosity (or distention), powder size and size distribution, thermomechanical response, and melting point. The condition of the powder surfaces is also important. The theory of Schwarz *et al.* [10] establishes the minimum pulse duration for consolidation. The shock pressure required for consolidation has been shown to be strongly dependent on the powder "hardness". Explosives with higher detonation velocities, which provide higher pressures, are required to consolidate harder powders. Most rapidly solidified powders fall in the latter category. These higher detonation-velocity explosives (composition B, TNT,

etc.) required to consolidate hard powders produce greatly increased fracturing and Mach stem formation. Staver [11] describes some alternative techniques for shock consolidation.

The approach described herein ensures high shock pressures while retaining a low detonation velocity which minimizes cracking and Mach stem formation. Conceptually, it is analogous to the use of a flyer plate to generate high pressures in plane-wave assemblies. Substantial improvements in the quality of consolidates was obtained by using the flyer tube technique. The experimental setup consists of two co-axial tubes, the external one being accelerated inwards and impacting the internal tube, that contains the powder. The pressures generated in the powder are several times higher than the one for the single-tube geometry, for the same quantity and type of explosive. In Section 2, the assembly will be briefly described and a simple "engineering " calculational procedure will be presented that permits the determination of the initial pressure in the powder. This calculation requires the establishment, first, of the equation of state for the powder. The pressures generated by a single tube and by a flyer tube will be estimated. Calculations will be conducted for a sample material, Inconel 718 powder. In Section 3, experimental results will be presented and discussed.

2. EXPERIMENTAL SET-UP AND PRESSURE CALCULATIONS

2.1. Set-up

The basic experimental set-up is shown in Fig. 1. It is similar to systems described previously in the literature [7]. The explosive charge is detonated at the top; a Detasheet booster is used to create a more uniform detonation front. The explosive is placed in the cylinder, at the center of which is the assembly containing the powder. The central axis of the container has a solid rod, to eliminate Mach stem formation. The difference between the system shown in Fig. 1 and conventional explosive consolidation systems is that a flyer tube is placed co-axially with the container tube. The utilization of a flyer tube has also been independently suggested by Wilkins [12] and implemented by Fujiwara [13].

2.2. Determination of equation of state for powder

In order to determine exactly the equation of state for a powder, instrumented gas-gun experiments have to be performed. However, reliable calculational procedures have been developed, and will be described here. McQueen *et al.* [14, 15], Altshuler [16], Mader [17], and Herrmann [18] used calculational procedures for the Hugoniots of shocked powders based on the Mie–Gruneisen equation, given by

$$P = P_H + \rho\gamma(E - E_H) \tag{1}$$

where P_H and E_H are the pressure and specific internal energy along the solid Hugoniot line in thermodynamic space and are functions of the specific volume, P and E are the pressure and specific energy for the porous material to be compacted; ρ is the density of the material. The Gruneisen ratio γ is assumed to be proportional to the specific volume: $\gamma/V = \gamma_0/V_0$ where γ_0 is the Gruneisen ratio at atmospheric pressure, and is expressed by the thermodynamic quantities

$$\gamma_0 = \frac{V_0 \beta K_0}{C_P}$$

where C_P is the specific heat at a constant pressure, K_0 is the isentropic bulk modulus, and β is the volumetric thermal expansion coefficient. Mader [17] approximated the γ_0 value as $(2S\text{-}1)$; S will be defined in the following paragraph. This approximation is used in the computations presented herein. The three equations for the conservation of mass, momentum, and energy (Rankine–Hugoniot relationships) are then applied to both the powder and the solid. For the solid, it is assumed that the particle velocity, u_H, is linearly related to the shock velocity U_H. In the equations below, the subscript H will be used when the parameter refers to the solid.

$$\rho(U_H - u_H) = \rho_0 U_H \tag{1}$$

$$P_H = \rho_0 U_H u_H \tag{2}$$

$$E_H = \frac{1}{2} P_H \left(\frac{1}{\rho_0} - \frac{1}{\rho}\right) \tag{3}$$

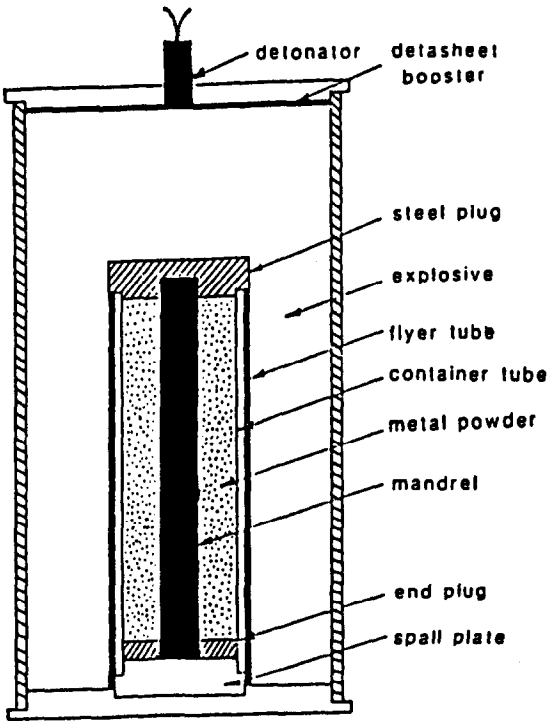

Fig. 1. Experimental set-up for consolidation using flyer tube technique; detonation is initiated at top and propagates downward accelerating flyer tube, which impacts metal container.

$$U_H = C + Su_H \tag{4}$$

$$\rho(U-u) = \rho_{00}U \tag{5}$$

$$P = \rho_{00}Uu \tag{6}$$

$$E = \frac{1}{2}P\left(\frac{1}{\rho_{00}} - \frac{1}{\rho}\right). \tag{7}$$

Expression (2) can be expressed as

$$P_H = \frac{C^2(V_0 - V)}{[V_0 - S(V_0 - V)]^2} \tag{8}$$

Inserting (3) and (8) into (1) leads to a relationship between P and V for the powder

$$P = \frac{[2V - \gamma(V_0 - V)]C^2(V_0 - V)}{[2V - \gamma(V_{00} - V)][V_0 - S(V_0 - V)]^2}. \tag{9}$$

For an equation expressing pressure as a function of particle velocity, V is obtained as a function of from equations (5) and (6) and incorporated into (9)

$$V = V_{00} - \frac{u^2}{P}. \tag{10}$$

Substituting (10) into (9)

$$\begin{aligned} &P^3\{2V_{00}[V_{00} - S(V_0 - V_{00})]^2 \\ &\quad - 2V_{00}C^2(V_0 - V_{00}) + \gamma C^2(V_0 - V_{00})^2\} \\ &\quad - P^2\{4V_{00}Su^2[V_{00} - S(V_0 - V_{00})] \\ &\quad + u^2(\gamma + 2)[V_{00} - S(V_0 - V_{00})]^2 \\ &\quad - C^2u^2[2(V_0 - V_{00}) - 2V_{00} \\ &\quad + 2\gamma(V_0 - V_{00})]\} + P\{2V_{00}S^2u^4 \\ &\quad + 2Su^4(\gamma + 2)[V_{00} - S(V_0 - V_{00})] \\ &\quad + C^2u^4(2 + \gamma)\} - S^2u^6(\gamma + 2) = 0. \end{aligned} \tag{11}$$

For a relationship between shock and particle velocities for the powder, equation (6) is substituted into equation (11). Since equation (11) is a third order equation, a simpler procedure is to solve equation (9) and find P–V pairs, applying them to equation (12), which is a combination of equations (5) and (6)

$$U = V_{00}\left(\frac{P}{V_{00} - V}\right)^{1/2}. \tag{12}$$

For obtaining particle velocities, one uses equation (13)

$$u = [P(V_{00} - V)]^{1/2}. \tag{13}$$

The constants C and S in the empirical equation $U_H = C + Su_H$ can be estimated from the experimentally determined values for pure elements [15, 19]. The simplest approach is to find C and S from the weighed average of weight fractions of principal constituents. For IN 718, one obtains C and S equal to 4.535 and 1.530, respectively.

The pressure vs particle velocity curves obtained by applying equations (9) and (13) for five different distentions are shown in Fig. 2(a). Figure 2(b) shows the pressure vs V/V_0 Hugoniot curves. It is worth noticing that the Mie–Gruneisen equation of state predicts volume increases at all pressures for a porosity of 50%. This aspect is discussed by Altschuler [16].

The energy deposited by the shock wave in the powder is an important parameter; it can be converted into an equilibrium shock temperature. Although this value does not describe the microscopic deformation phenomena at the particles it is a good estimate of the intensity of work done on the particles by the pressure pulse.

Figure 3(a) shows schematically how this energy is determined. From the definition [$E = 1/2P(V - V_0)$], the energy, at a pressure level P_H, is equal to the shaded areas for the solid and porous Hugoniot curves. This energy is larger for the powder than for the solid at the same pressure. These energies were determined as a function of pressure and porosity and are plotted in Fig. 3(b). Schwarz *et al.* [10] developed a direct equation to transform this energy into an upper bound for interparticle melting fraction, that will be used in Section 3.

2.3. Cracking and Mach stem formation

Cracking is a very significant problem in shock consolidation. Figure 4 shows the most common types of cracks observed in shock consolidated materials. These various types of cracks, as well as the techniques that are used to decrease or eliminate their occurrence, are discussed next.

(a) Circumferential cracks—they are produced by tensile pulse resulting from the reflection of the radially expanding compressive wave at the external wells of the cylinder. This is a spall fracture.

(b) Radial cracks—they are also produced by tensile tangential stresses. However, these are stresses that are insufficient to cause spalling and occur after the tensile pulse has traversed the specimen.

(c) Transverse cracks—transverse cracks are induced by (a) the tensile pulse produced by reflection of the compressive stress at the end of the specimen (after detonation has travelled its full course), (b) by stretching of the cylinder, and (c) by thermal stresses on cooling. If the total length of the cylinder is increased by virtue of longitudinal flow of material, a velocity differential is created in the cylinder. This velocity differential along the cylinder axis will establish stresses that can cause transverse cracking. Figure 5(a) shows the increase in length of the cylinder L produced by this effect. A velocity is imparted to the top surface of the compact. This gradient can produce substantial stresses. At a detonation velocity of 3000 m/s, an increase in length of 10 pct ($\Delta L/L_0$) will produce a velocity gradient of 300 m/s.

(d) Mach stem formation—a central hole is generated by the confluence of the shock waves at the center. The formation of the Mach stem is directly related to the angle α in Fig. 5(b). Here, one should adjust the experimental conditions to produce α as close as possible to 90°. At a certain initial level of pressure P_1 (required for consolidation of a material),

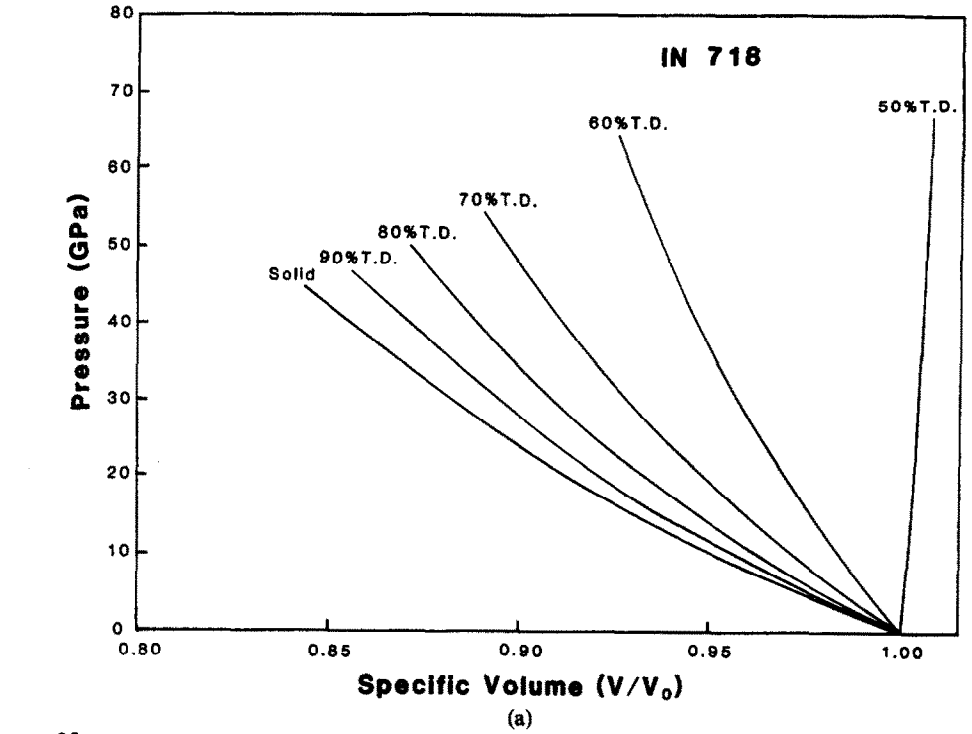

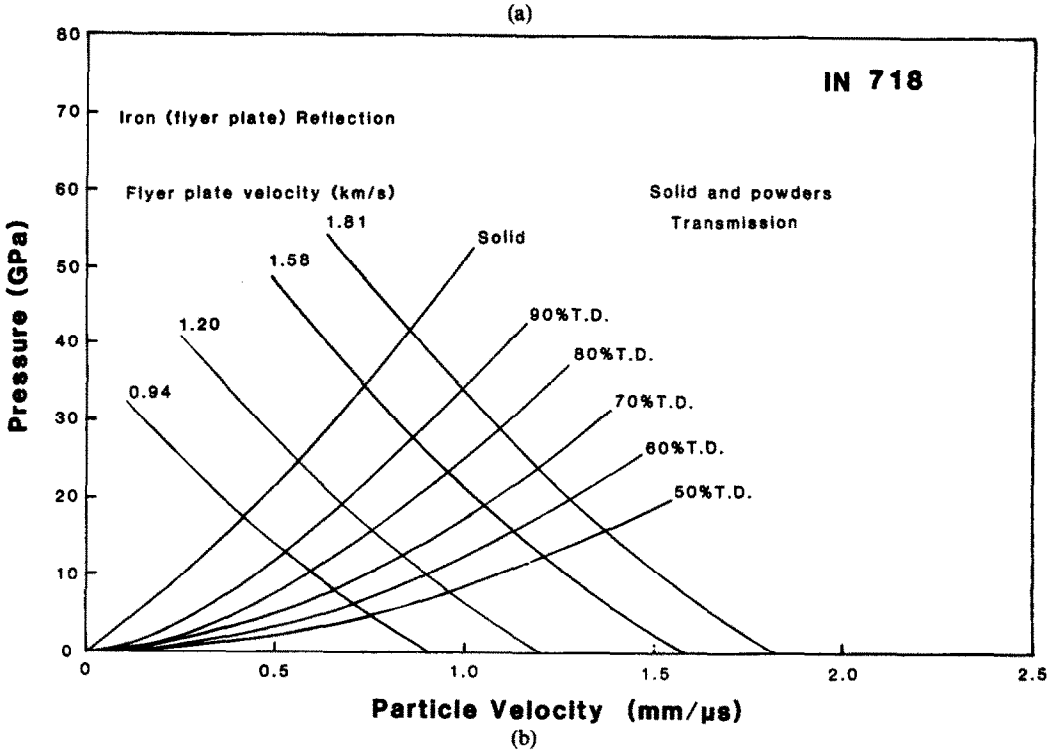

Fig. 2. (a) Calculated pressure–particle velocity curves for IN 718 powders of varying initial densities and reflected curves for iron for impedance matching calculations. (b) Calculated pressure–specific volume curve for IN 718 powders.

the lowering of the detonation velocity will change the configuration in Fig. 5(b) to that in Fig. 5(c); a front that is as planar as possible is desirable. The double-tube technique allows the use of low-detonation velocity explosives to produce high pressures. The pressure in the detonating explosive is given by $P = \rho_0 D^2/(\gamma + 1)$. Thus, increases in the Chapman–Jouguet pressures require increases in the detonation velocity. For the flyer tube technique, the pressure is dictated by the flyer-tube impact velocity that is determined by the kinetic energy transferred to the tube by the detonating explosive.

(e) Helicoidal cracks—helicoidal cracks are pro-

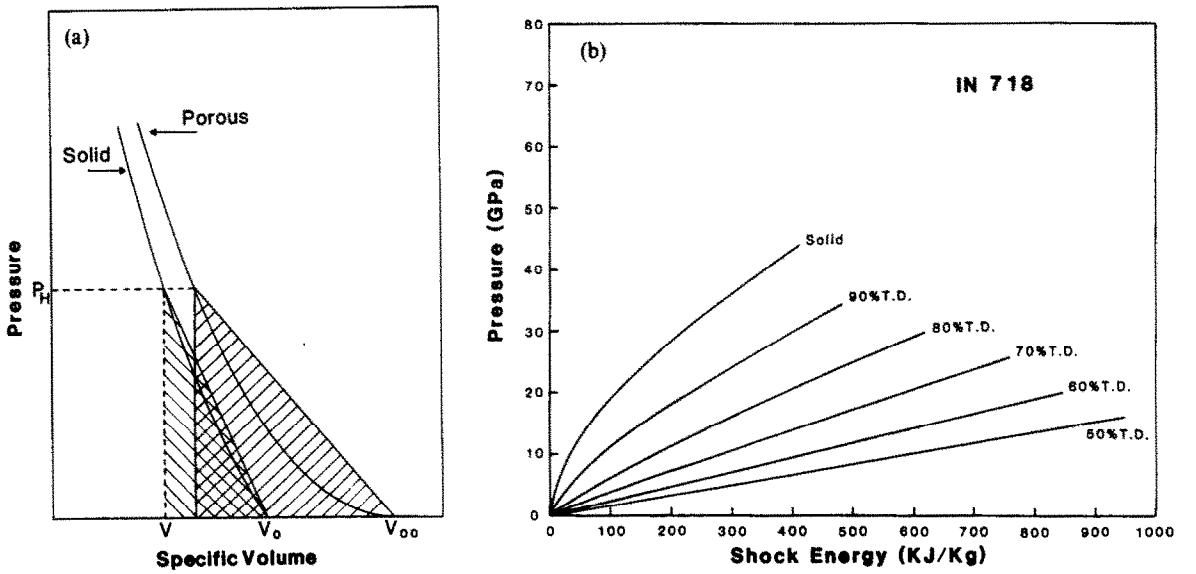

Fig. 3. (a) Schematic pressure–specific volume curves for solid and porous material. (b) Calculated pressure–shock energy for IN 718 powder at various distentions.

duced by compressive shear instabilities, as the diameter of the cylinder is reduced. Figure 6(a) shows the sequence of compaction. The outer regions are compacted first. As the shock-front propagates towards the center, the compacted material undergoes deformation, while the diameter is reduced to D_f. If the compacted material has sufficient ductility, this plastic deformation is accomodated uniformly. If ductility is not sufficient, cracking or shear localization along the surfaces of maximum shear stress will occur. This plane can be established by the simple stress analysis shown below. Referring to the stresses in Fig. 4, and assuming that the length of the cylinder is unchanged, one has

$$\epsilon_t = \epsilon_r = \frac{dr}{r} \quad \text{and} \quad \epsilon_l = 0. \tag{14}$$

Application of these equalities to the constitutive equations for elasticity yields

$$\sigma_r = \sigma_t \quad \text{and} \quad \sigma_l = 2\nu\sigma_r. \tag{15}$$

The maximum shear stress is thus

$$\tau_{max} = \frac{\sigma_r(1-2\nu)}{2} \tag{16}$$

The surface of maximum shear stress bisects the $x_l - x_t$ and $x_l - x_r$ planes [Fig. 6(b)]. This surface intersects the cross-section along a spiral, shown in Fig. 6(b). The propagation of these instabilities generates the helicoidal cracks.

If the material exhibits sufficient ductility, homogeneous plastic deformation accomodates the imposed detonation. The required ductility is calculated below.

From the initial and final volumes V_{00} and V_0, respectively, and assuming that the length of the cylinder remains constant, one has

$$\frac{V_{00}}{V} = \frac{D_0^2}{D_f^2}, \tag{17}$$

The plastic strain imposed on the outer layer of the cylinder is

$$\epsilon = \frac{\pi D_f - \pi D_0}{\pi D_0} = \frac{D_f}{D_0} - 1. \tag{18}$$

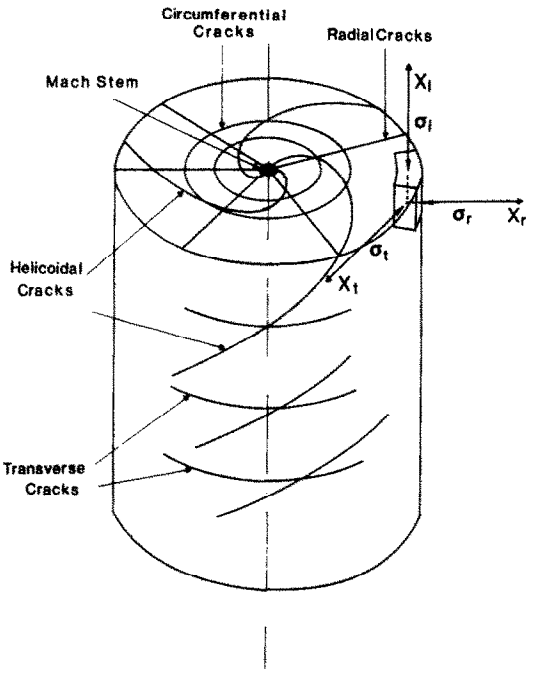

Fig. 4. Cracks and flaws encountered in shock consolidated cylinders.

Hence

$$\epsilon = \left(\frac{V_0}{V_{00}}\right)^{1/2} - 1. \tag{19}$$

For the example discussed in this paper where the initial powder density $\rho_{00} = 0.65\rho_0$, a ductility (in compression) of 0.225 is required for the avoidance of helicoidal cracks. Metallic glasses and ceramics do not possess this ductility at ambient temperature. Thus, solid cylinders cannot be shock compacted with this geometry at ambient temperature.

2.4. Calculation of tube velocity

Gurney [20] derived, in 1943, the classic equation for the velocity of fragments from bombs, shells, and grenades. In this equation, the chemical energy of the explosive is equated to the sum of the kinetic energy of the gases and that of the fragments. Some simplifying assumptions rendered this approach very straightforward; the most important is that the detonation product gases are assumed to have a linear velocity profile and a uniform density. The same assumptions, using the imploding cylinder geometry, are used here. An additional term, W_d, incorporating the energy expenditure in plastically deforming the tube from its initial radius r_0 to the final radius, r_f, is calculated. The tubes were invariably found to collapse symmetrically; no buckling was produced by the axysymmetric implosion. Figure 7(b) shows the linear velocity profile for the detonation gases. This implies

(a) at the time when all explosive has detonated

$$V_p = V_g \quad \text{at} \quad r = r_0 \tag{20}$$

(b) the gas velocity is a linear function with radius

$$V_g(r) = (V_p + V_0)\frac{r - R}{R - r_0} + V_0 \tag{21}$$

V_g is the velocity of gas products; V_p is the tube velocity; V_0 is the maximum velocity; R, r_0, and r are indicated in Fig. 7(a) and (b). Using the equation for conservation of momentum to solve for V_0 in terms of V_p

$$mV_p = \rho_e \int_{r_0}^{R} V_g \, dr \quad \text{where} \quad \rho_e = \frac{2r_0 C}{R^2 - r_0^2} \tag{22}$$

m and c are the areal densities of tube and explosive charge, respectively.

$$mV_p = \rho_e \int_{r_0}^{R} \left[(V_p + V_0)\frac{r - R}{R - r} + V_0\right] dr \tag{23}$$

$$V_0 = V_p\left[\frac{m(R^2 - r_0)}{c(Rr_0 - r_0^2)} + 1\right]. \tag{24}$$

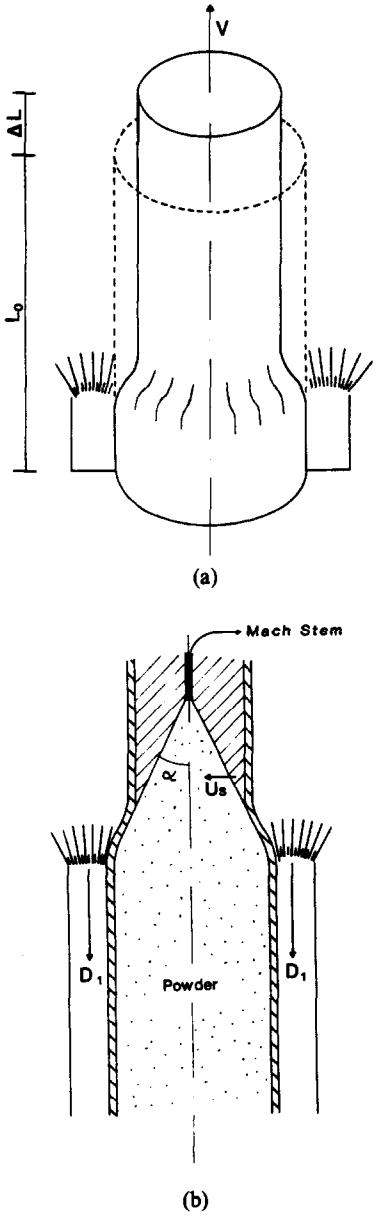

Fig. 5. (a) Velocity gradient induced in cylinder by lateral constriction. (b) Section of single-tube set-up. (c) Section of flyer-tube set-up.

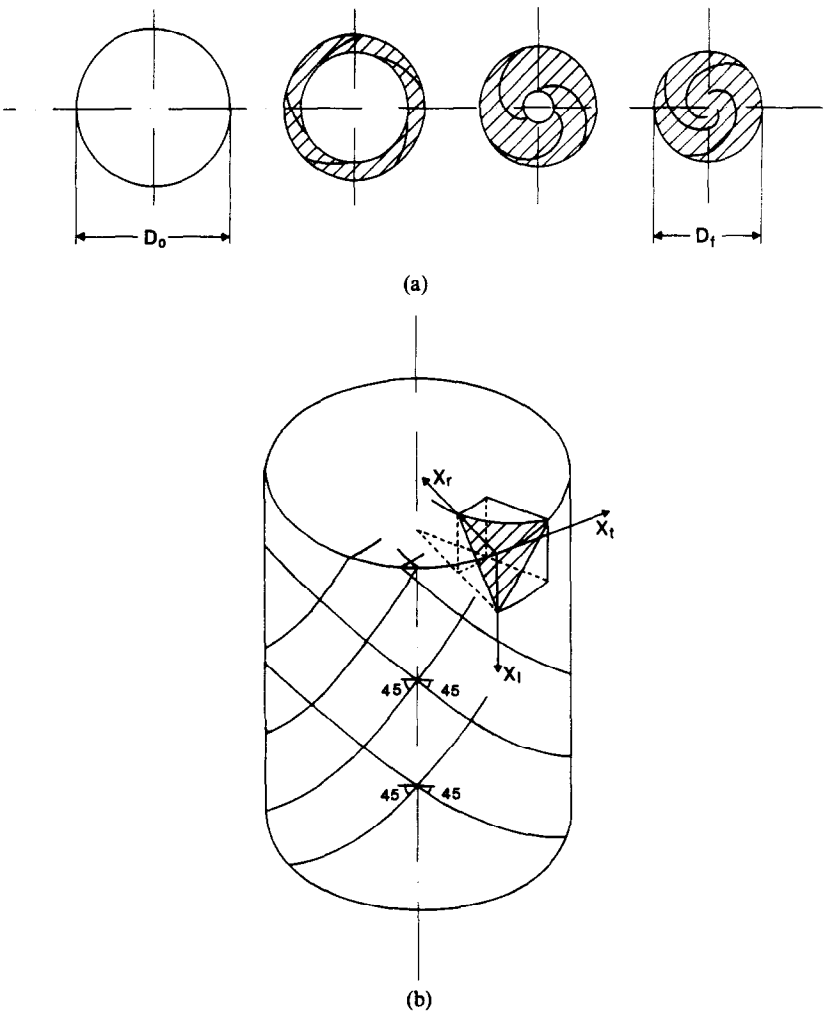

Fig. 6. Formation of helicoidal cracks in shock consolidation. (a) Cross-sections showing gradual reduction of diameter as compaction front propagates towards the cylinder axis. (b) Maximum shear stress surface and its intersection with the lateral surface of the cylinder.

Solving the equation for conservation of energy using the above V_0

$$E = \tfrac{1}{2} m V_p^2 + \frac{C r_0}{(R^2 - r_0^2)} \times \left[(R - r_0) \left(\frac{V_p^3}{3} - \frac{V_p V_0}{3} + \frac{V_0}{3} \right) \right] + W_d. \quad (25)$$

E is the Gurney energy (and is experimentally established); W_d, the energy expenditure in the plastic deformation of the cylinder, is calculated below. The length of the cylinder is assumed to be constant. Figure 7(c) shows the stresses imposed on an element in the cross-section of the tube. Assuming constancy of volume:

$$\epsilon_r = -\epsilon_\theta. \quad (26)$$

The flow stress of the tube material (AISI 1020 steel) will be assumed constant, and the plastic work is

$$dW_d = 2\sigma_r d\epsilon. \quad (27)$$

In the collapse of the tube, the diameter is reduced from r_1 (radius of powder container) to r_f, which are related by

$$\frac{r_1}{r_f} = \left(\frac{\rho_f}{\rho_0} \right)^{1/2}. \quad (28)$$

The initial radius r_0' is usually equal to $(r_1 + 2t)$. This assures a gap sufficiently large for acceleration prior to impact

$$r_f = (r_0' - 2t) \left(\frac{\rho_0}{\rho_f} \right)^{1/2}. \quad (29)$$

The total work on the element when the cylinder is imploded from r_0' to r_f is

$$W_d = \int_{r_0'}^{r_f} 2\sigma_r |d\epsilon_r| = \int_{r_0'}^{(r_0' - 2t)(\rho_0/\rho_f)^{1/2}} 2\sigma_d \left| \frac{dr}{r} \right| \quad (30)$$

where σ_d is the dynamic flow stress of the tube.

In the systems used in the present investigation, the powder had a density equal to 60 percent of the solid density, the internal diameter of the flyer tube was

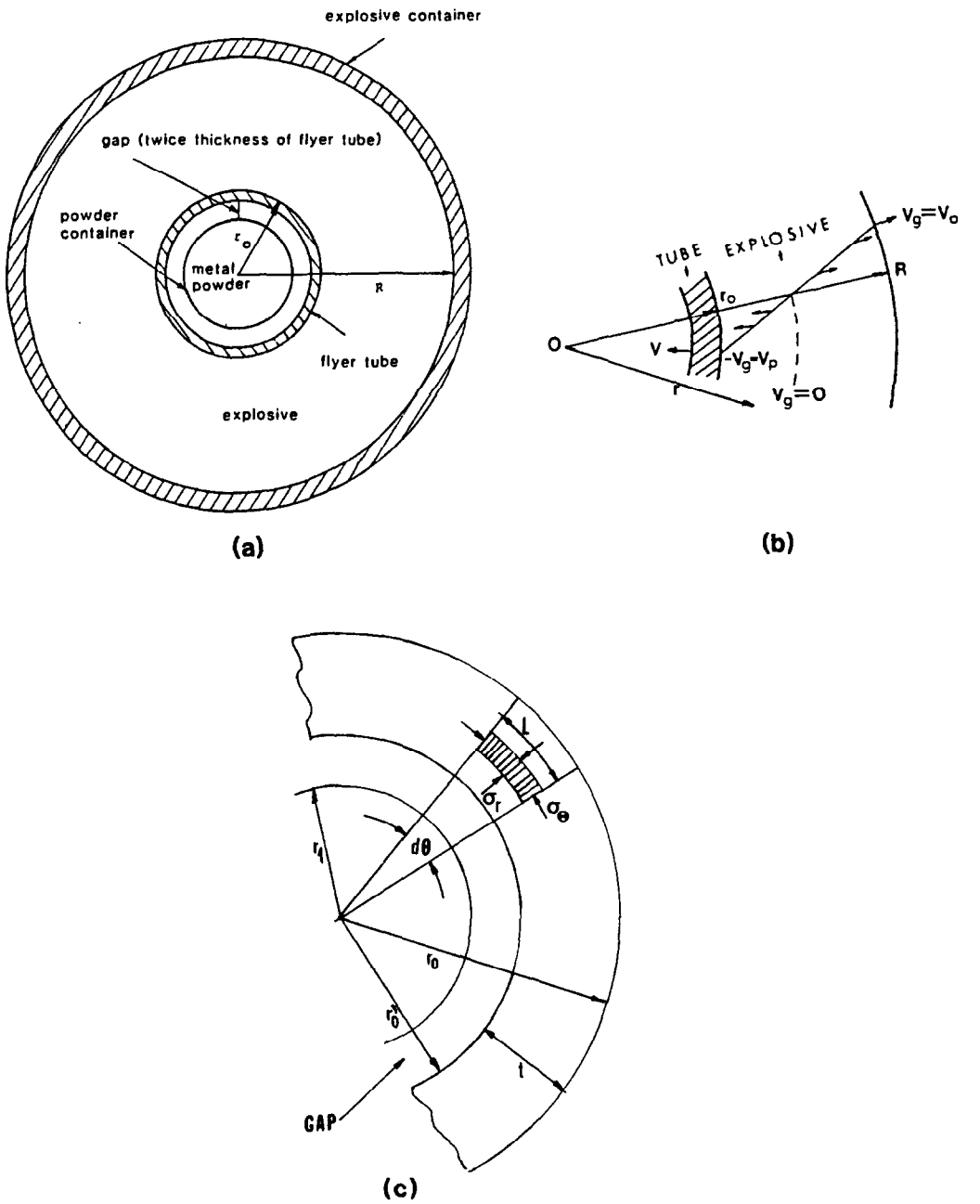

Fig. 7. (a) Cross-section of double-tube configuration. (b) Variation of velocity of gas with distance from flyer tube. (c) Elemental cube with radial and tangential stresses acting on it.

22.4 mm and the gap was 4 mm. From equation (29) it was found that r_f is equal to $0.63\,r_0'$.

Harding [21] reports a yield plateau of ~ 500 MPa for mild steel, at a strain rate of $1.75 \times 10^3\,s^{-1}$; Applying equation (30) one finds that W_d is equal to 1.27×10^5 N. In order to obtain an estimate of the order of magnitude of the plastic deformation work, it can be computed per unit mass. It is found to be equal to 18 J/g. By comparison, the Gurney energy of the explosive is of the order of 10^6 J/g. Hence W_d can, for most systems, be neglected. The last term in equation (25) is therefore dropped.

By rearranging terms

$$V_p = \sqrt{2E}\left[\frac{3}{5\left(\frac{m}{c}\right)+2\left(\frac{m}{c}\right)^2\frac{R+r_0}{r_0}+\frac{2r_0}{R+r_0}}\right]^{1/2}. \tag{31}$$

As expected this equation reduces itself to the well-known Gurney equation for open-faced sandwich

when R and $r_0 \to \infty$ (planar geometry)

$$V_p = \sqrt{2E}\left[\frac{3}{5\left(\frac{m}{c}\right)+4\left(\frac{m}{c}\right)^2+1}\right]^{1/2}. \quad (32)$$

Equation (31) allows the calculation of V_p, the tube velocity for a specific configuration. One factor not considered in the derivation is that the detonation is actually initiated at one end and that the detonation front propagates in a direction parallel to the cylinder axis. However, Lee and Pfeifer [22] found, through two-dimensional computer calculations, that tubular cylinders were driven to approximately the same terminal velocity if detonation was simultaneously initiated all along the axis or at one end.

Figure 8 shows the plot of the dimensionless velocity $(V_p/\sqrt{2E})$ of metal as a function of the loading factor (c/m). Once c/m is established, the value of $V_p/\sqrt{2E}$ can be determined. The quantity $V_p/\sqrt{2E}$ is known as the Gurney constant for a given explosive. The values of the Gurney energy for various explosives have been experimentally determined; Kennedy [23] gives values for several explosives. In Fig. 8, the predictions of equation (31) for an imploding cylinder are compared with predictions for an exploding cylinder (explosive charge placed in core of tube) and for a planar open-faced sandwich. It can be seen that the velocity rises faster for the imploding cylinder with c/m, beyond the value of c/m between 4 and 5, for which the three geometries give approximately the same velocity. The Gurney energy is not available for ANFO when detonation is non-ideal. Cooper [24] found that the Gurney constant of ANFO is equal to approximately one-third of the detonation velocity; this approximation was conducted at Sandia National Laboratories and gives good results.

2.5. Calculation of initial pressures for single and double tube geometrics

The computed initial pressures generated in Inconel 718 powder having 60 percent of the theoretical density will be conducted for the two configurations. This will be done for ANFO explosive using the impedance matching technique. The equations of state for various explosives are presented by Tanaka [25]. The detonation velocity of the explosive in the experiments conducted was found to be around 3100 m/s. Tanaka [25] gives values of the Chapman–Jouguet pressure and particle velocity as a function of explosive density. In the experiments conducted in the present investigation the detonation velocity did not reach the values for ideal detonation, and corrected values of the Chapman–Jouguet pressure and particle velocity had to be computed. This was done through the use of the equations

$$P_{CJ} = \frac{\rho_0 D^2}{\gamma + 1} \quad (33)$$

$$u_p = \frac{D}{\gamma + 1} \quad (34)$$

Where P_{CJ} and u_p are the Chapman–Jouguet pressure and particle velocity, D is the detonation velocity, and γ is the polytropic gas constant for the detonation products. The measured density of the ANFO explosive was 0.88 and Tanaka [25] reports $\gamma = 2.8$. From an average of the detonation velocities equal to 3,100 m/s, one computes a Chapman–Jouguet pressure of 2.2 GPa and a Chapman–Jouguet particle velocity of 814 m/s. The Hugoniot curve for ANFO was traced parallel to the Baratol curve passing through the (P_{CJ}, u_p) point. This is shown in Fig. 9. Using the impedance matching technique, one establishes the initial pressure in the powder. The procedure is described in greater detail by Kennedy [23]. An AISI 1010 container is used, and the Hugoniot curve for iron approximates it. Point 1 in Fig. 9 marks the pressure generated in the container (~8.3 GPa). The stress wave, upon entering the powder after passing through the container undergoes another change. At 1 the reflected Fe curve is passed through. This curve intersects the powder Hugoniot (Fig. 9) at a pressure of approximately 3 GPa. This is the initial pressure in the powder generated by the single tube assembly.

For the flyer tube assembly, one needs to use equation (31) to establish the flyer tube collapse velocity. The Gurney energy for ANFO can be approximated by taking it to be equal to one third the detonation velocity. This approximation is fairly accurate and was developed at Sandia [24]. For explosive containers of 15, 20, and 25 cm diameter, the plate velocities are found to be equal to be 0.94, 1.58, and 1.81 mm/μs. The impedance match technique can then be applied to this, as shown in Fig. 2(a). The reflected curves for the iron container are shown. The pressures generated in the powder are given by the intersection of these reflected iron curves, with origin at the plate velocities, with the

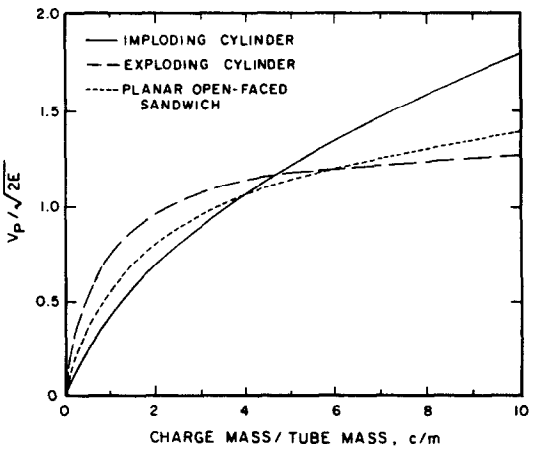

Fig. 8. Dimensionless velocity of metal as function of loading factor c/m for various geometries.

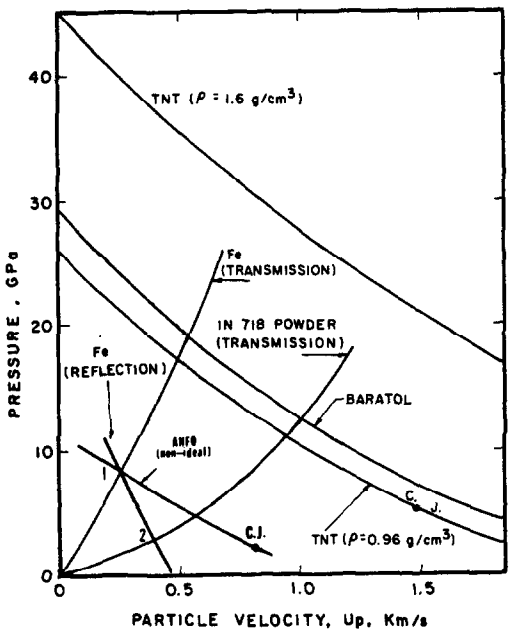

Fig. 9. Impedance match calculation for single-tube using ANFO (6% oil).

Inconel 718 powder curves. These pressures are equal to 8, 15, and 18 GPa for the 15, 20, and 25 cm ANFO containers, respectively. These pressures are much higher than the pressure generated by the single-tube geometry.

3. EXPERIMENTAL RESULTS

Experiments conducted on nickel-base superalloys and titanium alloys revealed the considerable differences in microstructure obtained using the two techniques. The microstructural changes were consistent with pressure differences calculated in Section 2.6. On a microscopic scale, interparticle melting, as evident from the white etching regions, is much more extensive for the flyer-tube than for the single-tube geometry. This can be evidenced by comparing Figs 10(a) and (b). The interparticle melt fractions (white pools) were determined by point counting.

The calculated and observed melting fractures are a function of pressure are shown in Fig. 11. The calculated values represent an upper bound and were obtained from Schwarz *et al.*'s [10] equation

$$L = \frac{P_1 V_0 (m-1)}{2[C_p(T_m - T_0) + H_m]} \qquad (35)$$

where L represents the ratio between the energy of the shock wave [values reported in Fig. 3(b)] and the energy required to bring a unit mass from the initial material to melt. m is the distention of the powder, C_p the heat capacity, T_m the melting point, T_0 the initial temperature and H_m is the heat of melting. This equation does not incorporate the energy expended in deforming the particles nor the thermal energy uniformly deposed by the shock wave.

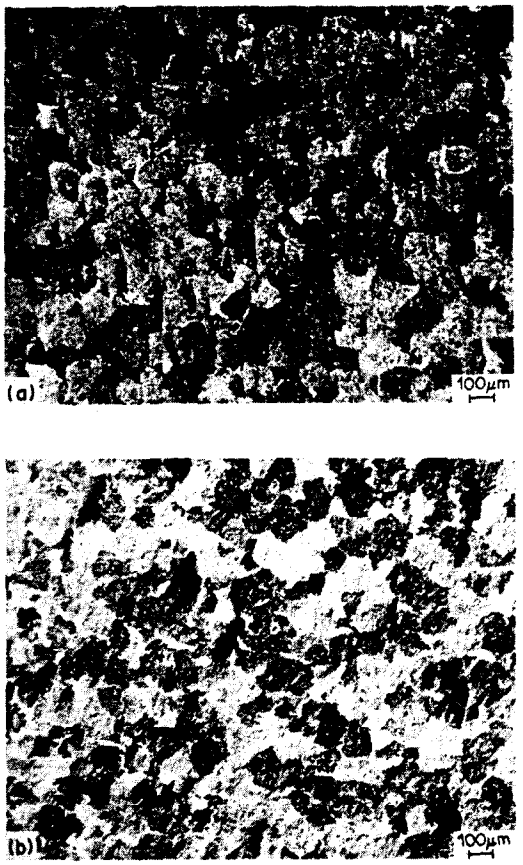

Fig. 10. Optical metallographs of (a) single-tube and (b) double-tube compactions.

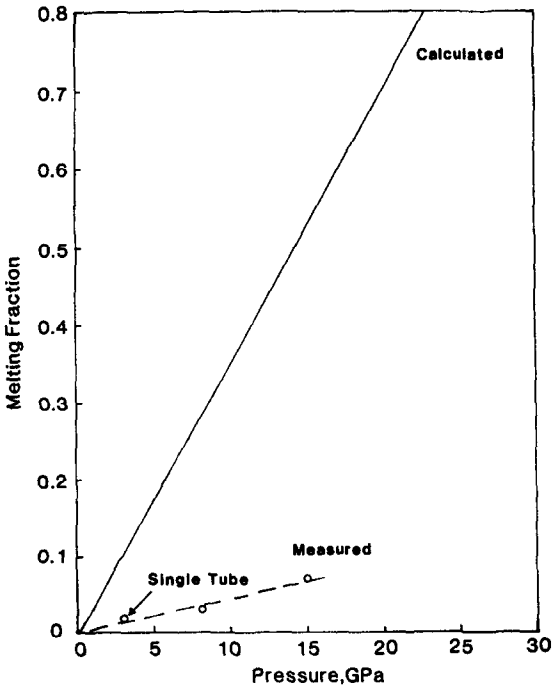

Fig. 11. Calculated and measured melting fractions as a function of pressure.

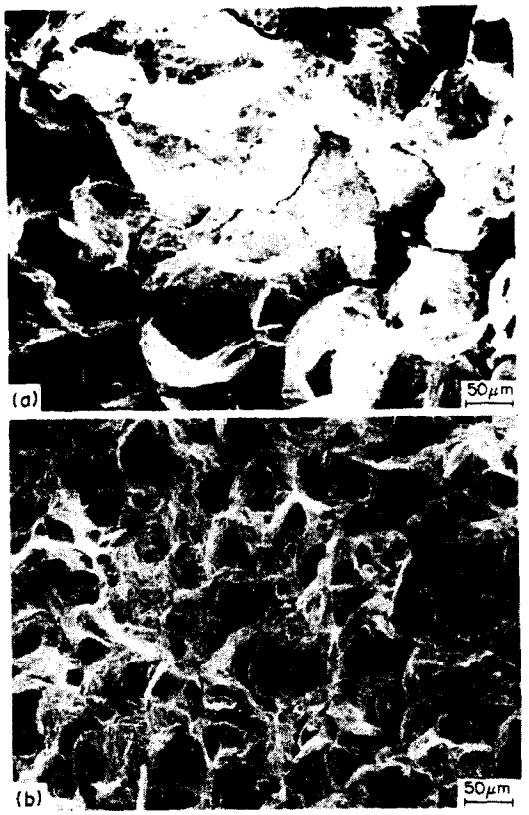

Fig. 12. Fracture surfaces of compact prepared by (a) single-tube geometry and (b) double-tube geometry.

The interparticle melting fractions predicted from equation (35) are therefore considerably larger than the ones observed experimentally, as is evident from Fig. 11. It is evident from Fig. 11 that the single-tube technique, generating a pressure considerably lower than the double tube technique, produces less melting. The interparticle melting fraction for the single-tube experiments was 0.02 while the interparticle melting fraction ranged from 0.06 to 0.09 for the flyer-tube assemblies. The fracture surfaces reveal the differences in consolidation. This is shown in Fig. 12. The specimen in the single-tube geometry consolidated poorly (in spite of compaction which closed virtually all pores) with weak interparticle bonding. This is evidenced by the fracture mode in which the particle boundaries are separated [Fig. 12(a)]. By contrast the fracture surface of Fig. 12(b) shows transparticle rupture, signifying that the bonding between the particles is at least as strong as the particles. This is a clear indication that the pressure was sufficient for consolidation.

Similar positive results were obtained upon consolidating Al–Li alloys and titanium alloys. The double-tube geometry produced good consolidation while minimizing cracking. Equation (31) was applied in determining the explosive load in scale-up of experiments. Figure 13 shows titanium alloy specimens shock consolidated. For the longest cylinder, weighing 20 lbs (100 N), approximately 100 lbs (500 N) of explosives were used. Scale-up was successful, showing that the equations are fairly realistic. One aspect of the double-tube shock consolidation technique not discussed previously is that it provides a square pulse with a sharp rise time.

4. CONCLUSIONS

A method for shock consolidation of metal powders is described. It produces pressures that are considerably higher than those in the single-tube geometry. This technique has yielded good consolidates of nickel-base superalloy IN 718, aluminum–lithium alloys, and titanium alloys. The technique lends itself well to scale-up, as shown in Fig. 13.

Acknowledgements—This work was supported by the Center for Explosives Technology Research and by General Electric Aircraft Turbine Division. The help of Dr M. Yoshida in the calculation of the equation of state for the powder is gratefully appreciated. Mr D. Brasher performed the calculations leading to the velocity of the imploding tube. Mr Dennis Hunter of TERA directed the shock consolidation experiments. Dr A. Szecket provided assistance and guidance in the initial stages of this investigation and in the implementation of the flyer-tube technique.

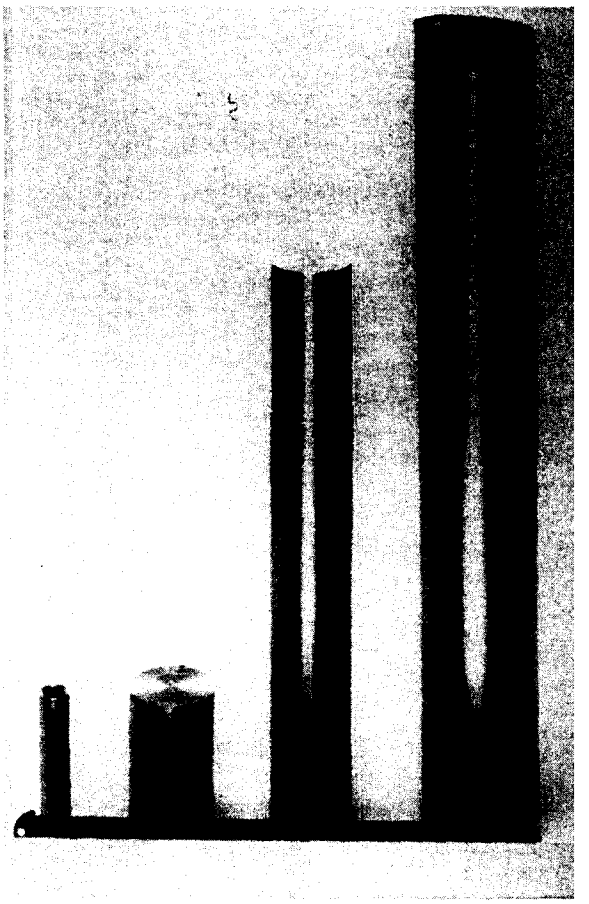

Fig. 13. Various cylindrical compacts prepared by flyer-tube method. (Scale in inches.)

REFERENCES

1. *Dynamic Compaction of Metal and Ceramic Powders.* NMAB-394 Natn. Acad. Sci. (1983).
2. M. A. Meyers and H.-r. Pak, *J. Mater. Sci.* **20,** 2133 (1985).
3. C. F. Cline and R. W. Hopper, *Scripta metall.* **11,** 1137 (1977).
4. D. Raybould, *J. Mater. Sci.* **16,** 589 (1981).
5. D. G. Morris, *Mater. Sci. Engng* **58,** 187 (1983).
6. W. H. Gourdin, *Prog. Mater. Sci.* **30,** 39 (1986).
7. R. Prummer, in *Explosive Welding, Forming and Compaction* (edited by Blazynski T. Z.), p. 369. Appl. Sci. Lond. (1983).
8. R. Prummer, *Explosivverdichtung Pulveriger Substanzen*, Springer, Berlin (1987).
9. S. L. Wang, M. A. Meyers and R. A. Graham, in *Shock Waves in Condensed Matter* (edited by Gupta Y. M.), p. 731. Plenum Press, New York (1986).
10. R. B. Schwarz, P. Kasiraj, T. Vreeland Jr and T. J. Ahrens, *Acta metall.* **32,** 1243 (1984).
11. A. Staver, in *Shock Waves and High-Stress-Rate Phenomena in Metals: Concepts and Applications* (edited by Meyers M. A. and Murr L. E.), p. 865. Plenum Press, New York (1981).
12. M. L. Wilkins, in *High Energy Rate Fabrication—1984* (edited by Berman I. and Schroeder J. W.), p. 63. Am. Soc. Mech. Engrs, New York (1984).
13. S. Fujiwara, Nat. Chem. Lab. for Industry, Tsukuba, Japan, personal communication (1985).
14. R. G. McQueen, S. P. Marsh, J. W. Taylor and W. J. Carter, in *Symp. on High Dynamic Pressure*, p. 67. IUTAM Paris, Gordon & Breach, New York (1968).
15. R. G. McQueen, S. P. Marsh, J. W. Taylor, J. M. Fritz and W. J. Carter, in *High Velocity Impact Phenomena* (edited by Kinslow R.), p. 293. Academic Press, New York (1970).
16. L. V. Altshuler, *Soviet Phys.* **8,** 52 (1965).
17. C. L. Mader, Los Alamos Scient. Lab. Rep. LA 4381 (1970).
18. W. Herrmann, *J. appl. Phys.* **40,** 2490 (1969).
19. M. A. Meyers, Ph.D. dissertation, Univ. of Denver, Colorado (1974).
20. R. K. Gurney, BRL Report 405 (1943).
21. J. Harding, in *Explosive Welding, Forming and Compaction* (edited by Blazynski T. Z.), p. 123. Appl. Sci. London (1983).
22. E. L. Lee and H. Pfeifer, UCRL Rep. 50545 (1969).
23. J. E. Kennedy, in *Behavior and Utilization of Explosives in Engineering Design* (edited by Henderson R. L.), p. 109. A.S.M.E. New Mexico, N.M. (1972).
24. P. W. Cooper, Sandia National Laboratories, personal communication, Albuquerque, N.M. (1986).
25. K. Tanaka, Detonation properties of condensed explosive computed using the Kihara–Hikita–Tanaka equation of state, Natn. Chem. Lab. for Industry, Tsukuba, Japan, p. 179 (1983).